Computational Modelling of Concrete Structures – Meschke, de Borst, Mang & Bićanić (eds)
© 2006 Taylor & Francis Group, London, ISBN 0 415 39749 9

Size effect on compression fracture of concrete with or without V-notches: a numerical meso-mechanical study

Gianluca Cusatis
Rensselaer Polytechnic Institute, Troy (NY), USA

Zdeněk Bažant
Northwestern University, Evanston (IL), USA

ABSTRACT: The present paper focuses on the analysis of the energetic size-effect on compression failure by adopting a recently developed three-dimensional lattice model for concrete. This model simulates the concrete mesostructure by an assembly of particles which are generated randomly according to the given grain size distribution of the coarse aggregates. Three-dimensional Delaunay triangulation generates the lattice mesh by connecting adjacent aggregates. A domain tessellation (similar to the Voronoi tessellation) defines the effective cross section areas of the connecting struts, which transmit both axial and shear forces according to a damage-type constitutive law. This constitutive law models fracture, friction and cohesion at the mesolevel. Numerical simulations of four sets of prismatic specimens scaled similarly in two dimensions with the ratios of 1:2:4:8 are carried out. The model parameters are preliminarily calibrated on the basis of available experimental data. For each set, both unnotched and notched specimens loaded under displacement control by non-rotating loading platens are considered. The numerical results are analyzed and the existence of size effect on both the strength and post-peak behavior in compression is proved.

1 INTRODUCTION

In recent years, several experimental and theoretical studies (see Burtscher and Kolleger (2004) and references therein) have brought attention to the problem of the size effect on the compression behavior of concrete, namely the dependence of the compressive nominal strength on the structural size. The current design practice, mainly based on plasticity concepts, disregards this phenomenon, which, on the contrary, is of great importance for the safety assessment of large structures such as skyscrapers, suspension bridges, and dams. The size effect can be statistical or energetic, or both. The statistical size effect is caused by the randomness of material strength as described by Weibull type theories. By contrast, the energetic size effect is caused by the fact that the rate of energy release into an advancing fracture tip scales with structure size, while the energy dissipated per unit area at the fracture tip is approximately independent of the structure size.

The present paper focuses on the analysis of the energetic size-effect on compression failure by adopting a recently developed three-dimensional lattice model for concrete. This model simulates the concrete mesostructure by an assembly of particles which are generated randomly according to the given grain size distribution of the coarse aggregates. Three-dimensional Delaunay triangulation generates the lattice mesh by connecting adjacent aggregates. A domain tessellation (similar to the Voronoi tessellation) defines the effective cross section areas of the connecting struts, which transmit both axial and shear forces according to a damage-type constitutive law. This constitutive law models fracture, friction and cohesion at the mesolevel. In this study numerical simulations of four sets of prismatic specimens scaled similarly in two dimensions with the ratios of 1:2:4:8 are carried out. For each set, both unnotched and notched specimens subjected to compressive loading are considered. The load is applied in displacement control by non-rotating loading platens.

2 ADOPTED CONSTITUTIVE LAW

The model used in the present study, called Confinement-Shear Lattice model (CSL model), simulates the concrete mesostructure by taking into account only coarse aggregates. A lattice mesh connecting the aggregate centers reproduces the interaction between adjacent aggregate pieces through the embedding matrix. The constitutive law assumed for each lattice element models the stiffness, strength and inelastic behavior, and includes the effect of the lower

level microstructure that is not directly introduced in the formulation (cement paste, small aggregate particles, cement-aggregate interface). In the following a review of the model formulation, whose detailed description appears in Cusatis et al. (2003a), Cusatis et al. (2003b), and Cusatis et al. (2005), is presented.

The geometry of the mesostructure for a given concrete specimen is obtained by using the following three-step algorithm to obtain. 1) A try-and-reject random procedure places each aggregate particle throughout the specimen volume. New randomly generated positions (coordinate triplets of particle centers) are accepted if they do not overlap with the previously placed particles and volume boundaries. In this step, zero-radius particles are also generated on boundary surfaces. 2) Delaunay tetrahedralization (Delaunay 1934; Barber et al. 1996) of the generated points defines the lattice mesh. Each tetrahedron edge represents a connecting strut between adjacent aggregate pieces. 3) A domain tessellation (dual complex of the Delaunay tetrahedralization) identifies the contact area through which the interaction forces are transmitted from one aggregate to the adjacent ones.

Rigid body kinematics describes the displacement field along the connection, while the displacement jump $[\![\mathbf{u}_C]\!]$ at the contact point, divided by the length L of the connection, defines the strain vector. The components of the strain vector in a local system of reference, characterized by the unit vectors $\mathbf{n}$, $\mathbf{l}$, and $\mathbf{m}$, are the normal and shear strains:

$$\varepsilon_N = \frac{\mathbf{n}^T[\![\mathbf{u}_C]\!]}{L}; \quad \varepsilon_L = \frac{\mathbf{l}^T[\![\mathbf{u}_C]\!]}{L}; \quad \varepsilon_M = \frac{\mathbf{m}^T[\![\mathbf{u}_C]\!]}{L} \tag{1}$$

The unit vector $\mathbf{n}$ is orthogonal to the contact area and the unit vectors $\mathbf{l}$ and $\mathbf{m}$ are mutually orthogonal and lie in the contact plane.

The normal stress σ_N and the shear stresses σ_L and σ_M are computed through a damage-like constitutive relation, which reads

$$\sigma_N = (1 - D)E\varepsilon_N \tag{2}$$

and

$$\sigma_i = \alpha(1 - D)E\varepsilon_i \quad (i = M, L) \tag{3}$$

where E is the elastic stiffness of the link, D is the damage parameter, α is the ratio of the tangential to the normal stiffness of the link. The damage parameter is defined as $D = 1 - \sigma/E\varepsilon$, in which $\sigma = [\sigma_N^2 + (\sigma_M^2 + \sigma_L^2)/\alpha]^{1/2}$ is the effective stress, and $\varepsilon = [\varepsilon_N^2 + \alpha(\varepsilon_M^2 + \varepsilon_L^2)]^{1/2}$ is the effective strain.

The evolution of the effective stress σ as a function of the effective strain ε is governed by the relations

$$\dot{\sigma} = E\dot{\varepsilon}, \quad 0 \le \sigma \le \sigma_b(\varepsilon, \omega) \tag{4}$$

where $\sigma_b(\varepsilon, \omega)$ is an exponential strain-dependent boundary simulating damage, fracture and plasticity at the mesolevel.

3 CALIBRATION OF THE MODEL PARAMETERS

The parameters of the model have been calibrated by fitting the response of concrete specimens under uniaxial compression reported in van Mier (1986). The reference properties of concrete are the following: cement content $c = 320\,\text{kg/m}^3$, water-cement ratio $w/c = 0.5$, aggregate-cement ratio $a/c = 6.0$, maximum aggregate size $d_a = 16\,\text{mm}$. The granulometric distribution has been obtained by an approximation of the classical Fuller curve: 5.8%, 11.5%, 12.7%, 11.3%, and 11.3% in mass of aggregates with characteristic size of 16 mm, 12.5 mm, 9.5 mm, 6.35 mm, and 4.75 mm, respectively. The optimized parameters defining the constitutive law (Cusatis et al. 2005) are $\alpha = 0.25$, normal elastic modulus of cement mortar $E_c = 30000\,\text{MPa}$, normal elastic modulus of aggregate $E_a = 3\,E_c$, tensile meso-strength (strength at mesolevel of microstructure) $\sigma_t = 3.0\,\text{MPa}$, tensile fracture energy at mesolevel $G_t = 0.03\,\text{N/mm}$, $\lambda_0 = 1.67 \cdot 10^{-4}$, meso-cohesion $\sigma_s = 3\sigma_t$, shear fracture energy $G_s = 30\,G_t$ compressive meso-strength $\sigma_c = 16\sigma_t$, hardening parameter at mesolevel $K_c = 0.26\,E_c$, shape parameter of compression cap $\beta = 1$, and slope of the hyperbola asymptote $\mu = 0.2$, $n_c = 2$.

The specimens are prisms with a constant cross section of $100 \times 100\,\text{mm}^2$ and three different heights: 50 mm, 100 mm and 200 mm. In the experiments, the load was applied under displacement control by a loading device that does not allow rotations of the loading platens during the tests.

Fig. 1 shows the best fitting of stress-strain curves for the three different specimens. The curves are normalized with respect to the peak stress (strength).

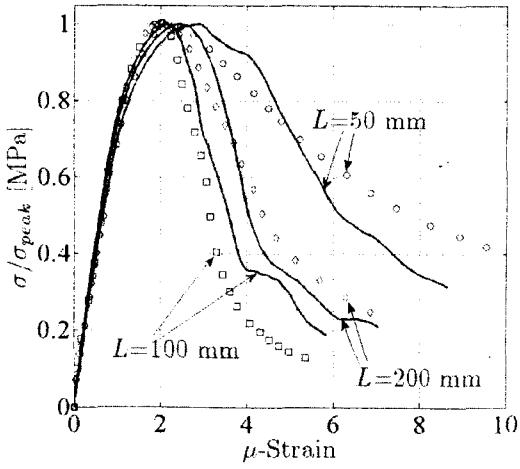

Figure 1. Best fitting of experimental data for parameter calibration.

The experimental and numerical average strengths are 42.05 MPa and 41.8 MPa, respectively. Note that each computed curve (solid lines) is the average of three curves obtained by computing the response of three specimens with different generated mesostructures.

4 SIZE EFFECT SIMULATIONS UNDER COMPRESSIVE LOADING

The simulated specimens are prisms of width D, length $L = 3D$, and thickness t. We consider four sets of prismatic specimen scaled similarly in two-dimension (with constant thickness $t = 50$ mm) characterized by $D = 50$ mm (small), 100 mm (medium), 200 mm (large), and 400 mm (extra-large). Each set is composed of 12 specimens with different random realizations of the mesostructure, i.e. with different aggregate positions. Fig. 2a shows a typical generated specimen for each characteristic size. The total number of aggregates (nodes) and the number of connections (lattice elements) are, respectively, 1235 and 7525 for the small specimen, 4022 and 25750 for the medium, 14355 and 94701 for the large, 54019 and 362409 for the extra-large. Fig. 2b shows typical notched specimens used in the calculations. The notches are V-shaped with an angle of 90 degrees and a depth equal to $D/4$.

The load is assumed to be applied under displacement control by a loading device that does not allow rotations of the loading platens during the tests. In addition, frictionless contact between the specimen ends and the loading platens has been assumed. The numerical simulations are carried out by an explicit dynamic algorithm.

Fig. 3a–d shows the nominal stress-strain curves obtained for the unnotched specimens. The nominal stress is defined as the applied load divided by the cross section area $A = tD$ of the specimen while the nominal strain is defined as the relative displacement of the loading platens divided by the length of the specimen. For the small size specimen, the behavior is linear elastic up to about 30% of the peak stress ($\approx$15 MPa) and the scatter between the twelve simulations is very limited. The scatter remains small also in the subsequent nonlinear range up to the peak. This phase is basically characterized by the development of diffuse microcracking in the entire volume of the specimen. As soon as the damage starts to localize and the micro-cracks tend to coalesce in a macro-crack the overall behavior becomes softening and the stress starts to decrease. The average peak stress is 41.3 MPa and the peak strain ranges from 2.5 to 3×10^{-3}. The post-peak behavior is characterized by the propagation of an inclined crack from the top left side of the specimen towards the bottom right side. The character of the damage localization and the subsequent fracture propagation is strongly influenced by the random nature of the mesostructure and, for this reason, the post-peak scatter of the various stress-strain curves increases significantly.

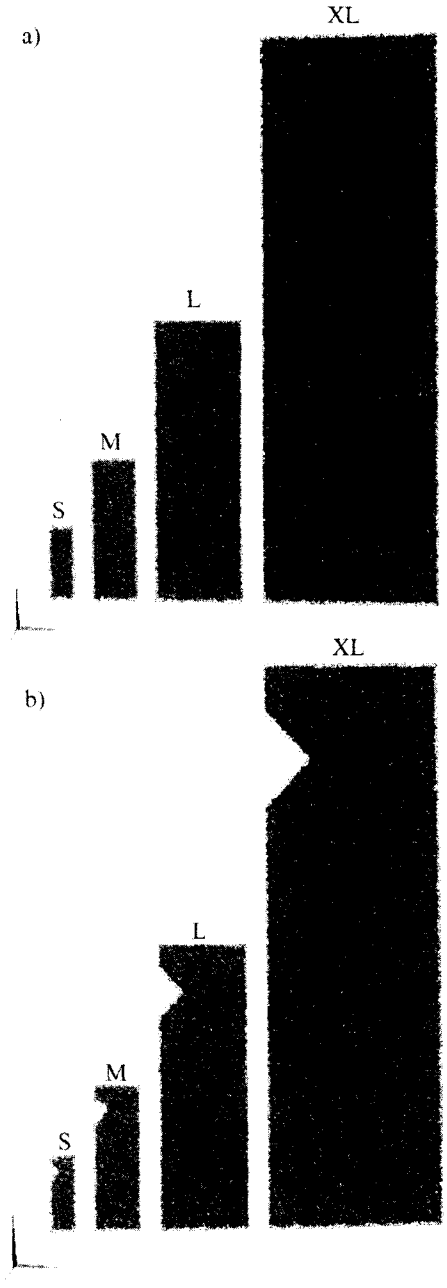

Figure 2. Geometry of the a) unnotched and b) notched specimens.

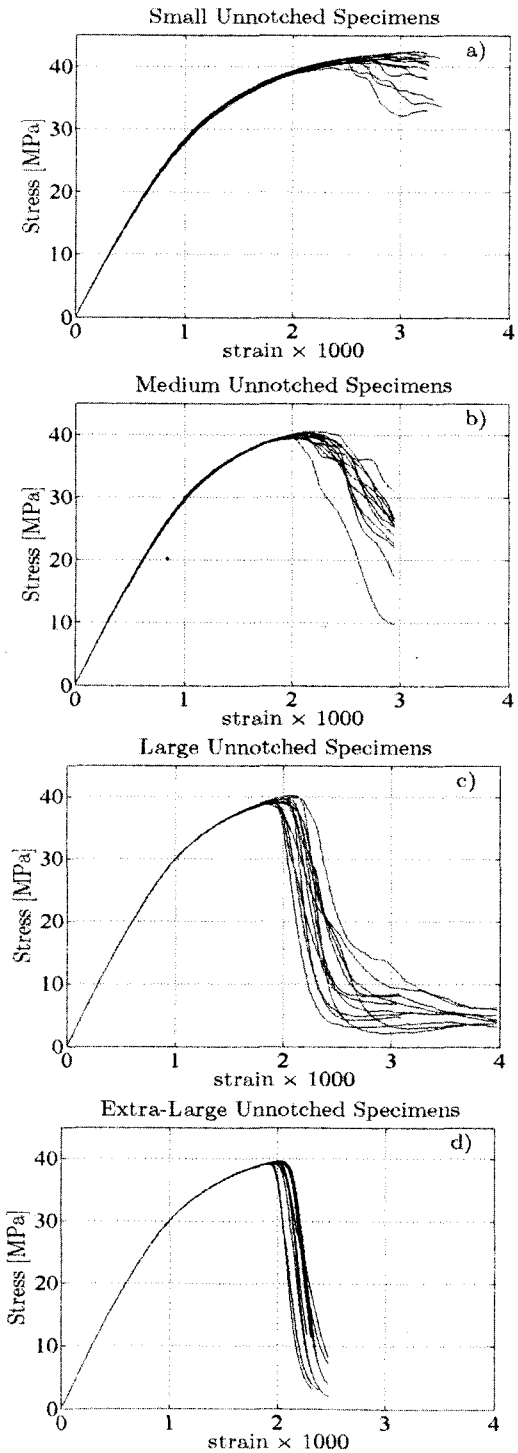

Figure 3. Stress-strain curves for unnotched specimens under compressive loading.

The stress-strain curves for the medium size specimens are presented in Fig. 3b. In this case the behavior is linear up to 50% of the peak load (≈20 MPa). Again the nonlinear behavior is characterized by diffuse damage at an early stage and by damage localization and macro-crack propagation in the post peak. The average peak stress is 40.0 MPa and the peak strain ranges from 2.0 to 2.3 × 10^{-3}. The average peak stress of the medium size specimens is about the same as the average peak stress of the small size specimens (only 3% less). Nevertheless, the post-peak is drastically different: the medium size specimens show a more brittle behavior. In the strain range from 2 to 3 × 10^{-3} the stress-strain curve of the small size specimens are still increasing or, in some cases, slightly decreasing (Fig. 3a). On the contrary, the curves in the same strain range for the medium size specimens are already softening, with a loss of load carrying capacity ranging from 20% to 80%.

The numerical simulations of the large size and extra-large size specimens confirm the trend just outlined. As the specimen size increases, the peak load remains about the same (39.4 MPa for both large and extra-large) but the behavior becomes more brittle. For the extra-large specimens the loss of load carrying capacity is sudden and the post-peak slope is almost vertical. A significant release of kinetic energy is associated with the vertical drop of the stress. This means that, had the loading process had been controlled by the crack opening, instead of the relative displacement of the loading platens, the stress-strain curves would have shown a snap-back.

The cause of the size effect on the post-peak slope of the stress-strain curves is energetic and it is associated with damage localization. As for the case of tensile fracture (Bažant and Oh 1983; Bažant 1984; Bažant and Planas 1997), the damage localizes in the the post-peak in a narrow band (Fig. 5b) while the rest of the material undergoes unloading. The width of the localization band is a material property and it does not scale similarly to the specimen geometry. This, in turn, implies that the dissipated energy and the released elastic energy scale proportionally to D^2 and D^3, respectively, leading to a more brittle behavior as the characteristic size D of the specimen increases.

The numerical results obtained for the notched specimens are plotted in Fig. 4a–d in terms of nominal stress-strain curves. The same definition of stress and strain as adopted in the case of unnotched specimens is retained here. For the small size specimens (Fig. 4a) the average peak stress is 35.2 MPa and the strain at peak ranges from 2 to 3 × 10^{-3}. For the medium size specimens (Fig. 4b) the average peak stress is 29.8 MPa, i.e., 15% lower than the peak stress for the small size specimens. Also the strain at peak is lower ranging from 1.2 to 1.8 × 10^{-3}. In the early stage of the nonlinear behavior, a diffuse micro-cracking evolution can be

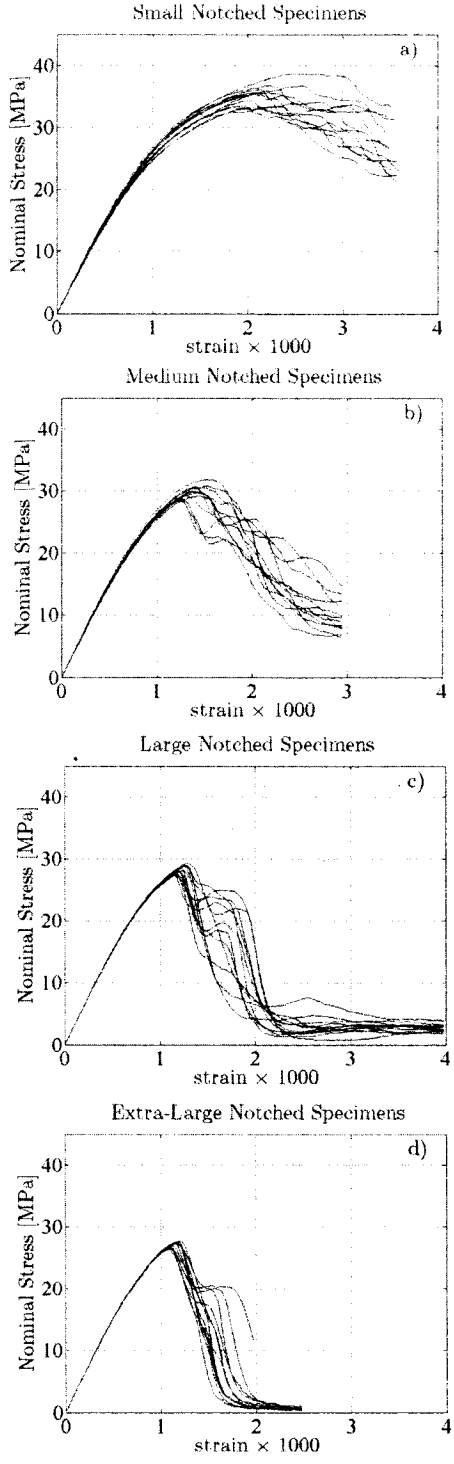

Figure 4. Stress-strain curves for notched specimens under compressive loading.

Figure 5. Typical amplified deformed shape at failure for a) notched and b) unnotched specimens.

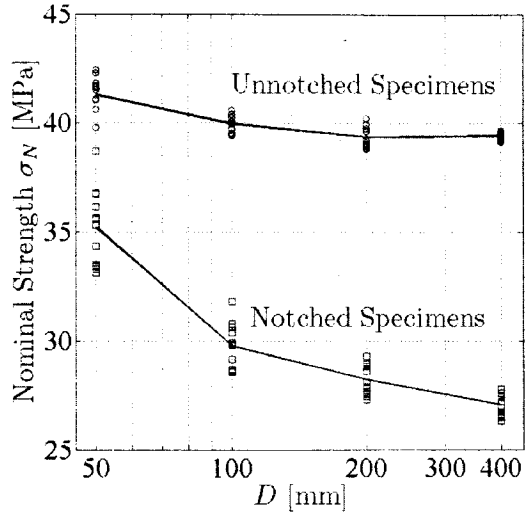

Figure 6. Size effect curves for unnotched (top) and notched (bottom) specimens subjected to compression.

observed in front of the notch tip. Similarly to what was previously observed for the unnotched specimens, an inclined macro-crack propagates also for the notched specimens only after the peak .

For the large and extra-large specimens (Fig. 4c, d), one can observe the same trend for the average peak stresses, 28.2 MPa and 27.0 MPa, respectively, and the strains at peak, 1.1–1.2 $\times 10^{-3}$ and 1.0–1.1 $\times 10^{-3}$,

respectively. As for the case of the unnotched specimens, the behavior tends to become more brittle as the characteristic size D increases. This again is due to damage localization, as can be clearly seen from Fig. 5a which shows a typical amplified deformed shape at failure for the case of notched specimens.

Fig. 6 shows the calculated size effect curves in log-log scales. Both curves are concave up, as it is expected because the peak load is attained at crack initiation (Bažant 2002).

5 CONCLUSIONS

The response of unnotched and notched specimens subjected to compressive loading has been numerically calculated by adopting a mesolevel lattice-type constitutive model. Four sets of geometrically similar specimens scaled in the ratios 1:2:4:8, have been analyzed. The following conclusions can be drawn:

1. The energetic size effect on compressive strength of concrete structures exists.
2. The size effect on compressive strength is significant in presence of notches but almost negligible for unnotched structures.
3. The size effect on compressive strength is of crack-initiation type (type I, (Bažant 2004)),
4. A strong size effect on the post-peak behavior is shown by both notched and unnotched structures.

ACKNOWLEDGMENTS

The support of this work by DoT under grant 0740-357-A497 from Infrastructure Technology Institute of Northwestern University is gratefully acknowledged.

REFERENCES

Barber, C., D. Dobkin, and H. Huhdanpaa (1996). The Quick-hull algorithm for convex hulls. *ACM Trans Math Softw 22*(4), 469–483. http://www.qhull.org.

Bažant, Z. (2004). Scaling theory for quasibrittle structural failure. *Proc., National Academy of Sciences 101*(37), 1339713399. Inaugural article.

Bažant, Z. and J. Planas (1997). *Fracture and size effect in concrete and other quasibrittle materials* (W. F. CHEN ed.). New directions in civil engineering. CRC Press.

Bažant, Z. P. (1984). Size effect in blunt fracture: concrete, rock, metal. *J. Engrg. Mech., ASCE 110*(4), 518–535.

Bažant, Z. P. (2002). *Scaling of Structural Strength*. Hermes Penton Science (Kogan Page Science). 2nd updated edition, Elsevier 2005, London.

Bažant, Z. P. and B. H. Oh (1983). Crack Band Theory for Fracture of Concrete. *Matériaux et Constructions 16*, 155–177.

Burtscher, S. L. and J. Kolleger (2004). Size effect experiments on granular materials in compression. In L. et al. (Eds.), *Fracture Mechanics of Concrete Structures*, pp. 173–180. Ia-FraMCos.

Cusatis, G., Z. Bažant, and L. Cedolin (2003a). Confinement-shear lattice model for concrete damage in tension and compression: I. theory. *J of Engrg Mech, ASCE 129*(12), 1439–48.

Cusatis, G., Z. Bažant, and L. Cedolin (2003b). Confinement-shear lattice model for concrete damage in tension and compression: II. computation and validation. *J of Engrg Mech, ASCE 129*(12), 1449–58.

Cusatis, G., Z. Bažant, and L. Cedolin (2005). Confinement-shear lattice csl model for fracture propagation in concrete. *Comput. Methods Appl. Mech. Engrg.* In press.

Delaunay, B. (1934). Sur la sphère vide. *Bull Acad Sci USSR(VII), Classe Sci Mat Nat*, 793–800.

van Mier, J. G. M. (1986). Multiaxial strain-softening of concrete. Part I: Fracture. *Materials and Structures 19*, 179–190.